AD-A183 200 SMALL-SCALE CRACK BRIDGING AND THE FRACTURE TOUGHNESS OF PARTICULATE-REIN.. (U) HARVARD UNIV CAMBRIDGE MA DIV OF APPLIED SCIENCES B BUDIANSKY ET AL. JUN 87 MECH-104 1/1

UNCLASSIFIED N00014-86-K-0753 F/G 11/2 NL

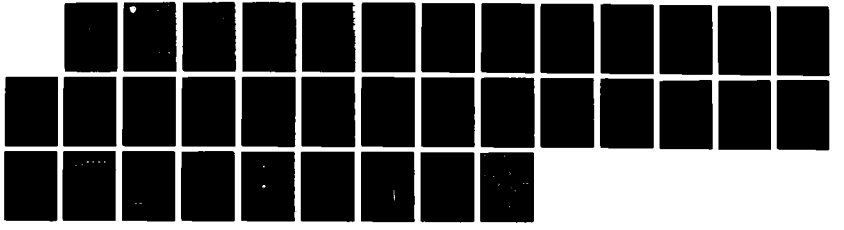

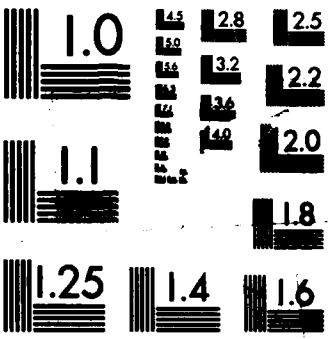

MICROCOPY RESOLUTION TEST CHART
NATIONAL BUREAU OF STANDARDS-1963-A

MECH-104

SMALL-SCALE CRACK BRIDGING AND THE FRACTURE TOUGHNESS OF PARTICULATE-REINFORCED CERAMICS

Contract N00014-86-K-0753

Bernard Budiansky, John C. Amazigo and Anthony G. Evans

Division of Applied Sciences
HARVARD UNIVERSITY
Cambridge, Massachusetts 02138

June 1987

SMALL-SCALE CRACK BRIDGING AND THE FRACTURE TOUGHNESS OF PARTICULATE-REINFORCED CERAMICS

by
Bernard Budiansky and John C. Amazigo*
Division of Applied Sciences
Harvard University
Cambridge, MA 02138
and
Anthony G. Evans
Materials Department, College of Engineering
University of California
Santa Barbara, CA 93106

ABSTRACT

Theoretical analyses of small-scale bridging of crack surfaces by elastic-ideally plastic springs are presented and applied to the study of the fracture toughness of ceramics reinforced by small particles. The dependence of toughening on particle size, concentration, strength, and ductility is explored, and relations between toughening and bridge length at fracture are given. Available experimental information is examined in the light of the analyses. Keywords: particulate toughening; metal reinforced ceramics.

INTRODUCTION

The fracture toughness of a composite consisting of a ceramic matrix containing ductile metal particles is studied theoretically in this paper on the basis of the hypothesis (e.g. Krstic 1983) that the metallic inclusions toughen the ceramic by the mechanism of *crack-bridging* (Fig. 1). It is presumed that the faces of an advancing crack in the ceramic are pinned together by intact particles for some distance behind the crack tip, reducing the crack-tip stress intensity that would otherwise occur. The length of the bridged zone and the amount of toughening that occurs depend on the breaking strength of the particles, as well as on the deformations they may undergo before they fail. Clearly, for crack-bridging to be effective a matrix crack should

---

* On Sabbatical Leave from the Department of Mathematics, University of Nigeria, Nsukka, Nigeria.

tend to be attracted to the particles, and it would appear that a necessary condition for this to occur is that the elastic stiffness of the particles be less than that of the matrix.

In a preliminary outline of some of the present results (Budiansky 1986) a *bridging-spring* model (Fig. 2) for the partially pinned crack was described. The same model has recently received extensive mathematical study from Rose (1986), who cites a variety of fracture problems to which the model has relevance. In this paper we limit our attention to the case of *small-scale bridging*, in which bridge length is small relative to crack length, specimen dimensions, and distances from the crack to the specimen boundaries. We discuss the associated bridging-spring equations and their solutions, and then consider the implications of these solutions with respect to the problem of particulate reinforcement.

BRIDGING-SPRING MODEL

Elastic springs

In the absence of springs connecting the faces of the plane-strain, Mode-I crack shown in Fig. 2, the stresses near the crack tip would have the standard distribution

$$\sigma_{\alpha\beta} \sim K f_{\alpha\beta}(\theta)/(2\pi r)^{1/2} \tag{1a}$$

where K is the stress intensity factor. In accordance with the assumption of small-scale bridging, we will study the effects of the springs by letting the crack be infinitely long, and assume that the distribution (1a) is approached asymptotically for $r \to \infty$. The crack-tip stress distribution will then become

$$\sigma_{\alpha\beta} \sim K_m f_{\alpha\beta}(\theta)/(2\pi r)^{1/2} \tag{1b}$$

for $r \to 0$. We intend to calculate the new stress-intensity factor K_m and the spring forces in terms of the "applied" stress-intensity factor K, the bridge-length L, and the spring characteristics. For the case of linear springs we adopt the notation of Rose (1986) here, and write the spring stress as

$$\sigma = kEv/(1-\nu^2) \tag{2}$$

in terms of the crack-face displacement v, Young's modulus E, Poisson's ratio ν, and a spring-stiffness coefficient k. A relation connecting K_m, K, and the stress $\sigma(L)$ at the end of the bridged zone follows immediately from the use of the Rice (1968) J-integral

$$J = \int_\Gamma (W n_1 - \sigma_{\alpha\beta} u_{\alpha,1} n_\beta) ds = 0 \tag{3}$$

taken around the path shown in Fig. 3. (Here W is the strain-energy density and u_α is the displacement vector; the horizontal parts of Γ lie just outside the line of springs.) The result

$$\frac{(1-\nu^2)K^2}{E} = \frac{(1-\nu^2)K_m^2}{E} + \frac{(1-\nu^2)\sigma^2(L)}{kE} \tag{4}$$

(Rose 1986, Budiansky 1986) provides an equation for the *toughening ratio* $\lambda = K/K_m$, in the following sense. Suppose K_m represents the critical stress-intensity factor for crack growth in the matrix, and imagine that new springs connecting the crack faces emanate from the crack tip whenever the crack propagates. Then, if we set the peak spring stress $\sigma(L)$ equal to the spring breaking-strength σ_Y, crack propagation with simultaneous fracture of the last spring will occur for

$$\lambda = \left[1 + \frac{\sigma_Y^2}{kK_m^2}\right]^{1/2} \tag{5}$$

The J-integral relation (4) has an energetic interpretation. During the propagation process just described, energy is released into the crack tip at a rate (per unit crack advance) given by the first term on the right, and the second term is the energy loss rate caused by fracture of the last spring. The left side, therefore, represents the energy input rate provided by the applied field.

We would also like to find the relation between λ and the bridge length L, and for this purpose we will have to determine the spring stress distribution $\sigma(x)$. A convenient starting point is to write the integral equation

$$\frac{(1-\nu^2)\sigma(x)}{kE} = \frac{4(1-\nu^2)K\sqrt{x}}{E\sqrt{2\pi}} - \frac{4(1-\nu^2)}{\pi E}\int_0^L \sigma(x')\log\left(\frac{\sqrt{x}+\sqrt{x'}}{\sqrt{|x-x'|}}\right)dx' \tag{6}$$

for $\sigma(x)$ in (0,L). The left side is the crack-face displacement given by (2) in terms of the spring stress; the terms on the right are the displacement due to the applied K-field (1a), and the reduction of this displacement due to the action of the spring forces on the crack faces (Tada et al., 1985). The substitutions

$$s = \frac{4kx}{\pi}, \quad t = \frac{4kx'}{\pi}, \quad g = \frac{\sigma}{K\sqrt{2k}} \tag{7}$$

give

$$g(s) + \int_0^\alpha g(t)\log\left(\frac{\sqrt{s}+\sqrt{t}}{\sqrt{|s-t|}}\right)dt = \sqrt{s} \tag{8}$$

where

$$\alpha = \frac{4kL}{\pi} \tag{9}$$

It follows from (4) that the ratio $\lambda = K/K_m$ is given by

$$\lambda = [1-2g^2(\alpha)]^{-1/2} \tag{10}$$

The numerical solution of the integral equation (8) for g(s) is described in detail in Appendix A. The results for λ given by Eq.(10) are shown in Table I for values of α in the range (0,30), and a plot of λ versus α is given by the top solid curve in Fig. 4.

A check on the numerical accuracy of the results was provided by another formula connecting λ and g(s) that follows from the relation (Tada et al., 1985)

$$K_m = K - \sqrt{\frac{2}{\pi}}\int_0^L \frac{\sigma(x)}{\sqrt{x}}dx \tag{11}$$

which gives

$$\lambda = \left[1 - \int_0^{\alpha} \frac{g(s)ds}{\sqrt{s}} \right]^{-1} \tag{12}$$

A direct proof that the J-integral formula (10) is consistent with (12) and the integral equation (8) is given in Appendix B. The results for λ given by the formulas (10) and (12) were in excellent agreement with each other, and also with those found by Rose (1986) by a different procedure.

Since $g(s) \approx \sqrt{s}$ for small α, it follows that $\lambda \approx (1+\alpha)$ for $\alpha \to 0$. Also, for $\alpha \to \infty$, Rose has demonstrated the asymptotic relation

$$\lambda \approx \pi\sqrt{\alpha/2} \tag{13}$$

The results for the non-dimensional spring stress $g \equiv g(s;\alpha)$ are plotted in Fig. 5 against the non-dimensional distance $(\alpha-s)$ from the "last" spring, for $\alpha = 2$, 5, and 20. Also shown for comparison are the results for g given by a Wiener-Hopf solution for the limiting case $\alpha=\infty$ (Budiansky 1986, Rose 1986), summarized briefly in Appendix C. Note that g(s) peaks sharply at $s=\alpha$, consistent with the behavior

$$g'(s) \approx -\frac{g(\alpha)}{2} \log(\alpha - s) \tag{14}$$

for $s \to \alpha$ that follows from Eq.(8).

The model will now be extended to the case of elastic-plastic springs, in order to provide a basis for the study of particulate toughening when plastic yielding of the particles is important.

Elastic-plastic springs

We assume now that for increasing v, the springs obey the elastic-ideally plastic constitutive relation

$$\sigma = kEv/(1-\nu^2) \qquad \text{for } v \le v_Y \equiv \frac{\sigma_Y(1-\nu^2)}{kE}$$

$$= \sigma_Y \qquad \text{for } v \ge v_Y \tag{15}$$

Then if v(L) at the end of the bridged zone exceeds v_Y, the J-integral result (4) generalizes to

$$\frac{(1-\nu^2)K^2}{E} = \frac{(1-\nu^2)K_m^2}{E} + \frac{(1-\nu^2)\sigma_Y^2}{kE} + 2\sigma_Y[v(L) - v_Y] \tag{16}$$

If failure of the last spring is now presumed to occur when $[v(L) - v_Y]$ attains a critical plastic value v_P, then the toughening ratio becomes

$$\lambda = \left[1 + \frac{\sigma_Y^2}{kK_m^2}\left(1 + \frac{2v_P}{v_Y}\right)\right]^{1/2} \tag{17}$$

If plastic yielding ($v > v_Y$, $\sigma = \sigma_Y$) occurs for $L_Y < x < L$, the spring stress distribution in $(0,L_Y)$ is governed by

$$\frac{(1-\nu^2)\sigma(x)}{kE} = \frac{4(1-\nu^2)K\sqrt{x}}{E\sqrt{2\pi}} - \frac{4(1-\nu^2)}{\pi E}\int_0^{L_Y} \sigma(x')\log\left(\frac{\sqrt{x}+\sqrt{x'}}{\sqrt{|x-x'|}}\right)dx'$$

$$-\frac{4(1-\nu^2)}{\pi E}\sigma_Y\int_{L_Y}^{L} \log\left(\frac{\sqrt{x}+\sqrt{x'}}{\sqrt{|x-x'|}}\right)dx' \tag{18}$$

In non-dimensional form (see (7)) this is

$$g(s) + \int_0^{\alpha_Y} g(t)\log\left(\frac{\sqrt{s}+\sqrt{t}}{\sqrt{|s-t|}}\right)dt + g_Y\int_{\alpha_Y}^{\alpha} \log\left(\frac{\sqrt{s}+\sqrt{t}}{\sqrt{|s-t|}}\right)dt = \sqrt{s} \qquad (0 \le s \le \alpha_Y) \tag{19}$$

where

$$\alpha_Y = 4kL_Y/\pi\ ,\ g_Y = g(\alpha_Y) \tag{20}$$

The solution of (19) for prescribed values of α and α_Y is described in Appendix A. The associated values of v_P/v_Y follow from the fact that $v(L) = v_P + v_Y$ is given by the right-hand side of (18) evaluated at x=L. Hence

$$v_P/v_Y = -1 + \frac{1}{g_Y}\left[\sqrt{\alpha} - \int_0^{\alpha_Y} g(s)\log\left(\frac{\sqrt{\alpha}+\sqrt{t}}{\sqrt{|\alpha-t|}}\right)dt\right] - \int_{\alpha_Y}^{\alpha} \log\left(\frac{\sqrt{\alpha}+\sqrt{t}}{\sqrt{|\alpha-t|}}\right)dt \qquad (21)$$

and the corresponding value of λ follows from (17) as

$$\lambda = \left[1 - 2g_Y^2\left(1 + 2\frac{v_P}{v_Y}\right)\right]^{-1/2} \qquad (22)$$

A check is provided by the formula

$$\lambda = \left[1 - \int_0^{\alpha_Y} \frac{g(s)}{\sqrt{s}}ds - 2g_Y\left(\sqrt{\alpha} - \sqrt{\alpha_Y}\right)\right]^{-1} \qquad (23)$$

that follows from (11).

The previously discussed results for elastic springs correspond to $\alpha_Y=\alpha$ and $v_P/v_Y=0$. By varying α_Y at given values of α, solutions were found, by interpolation, for a number of prescribed values of v_P/v_Y. The results for λ versus α are shown in Fig. 4.

Rigid-plastic springs

In the limit of very large v_P, the elastic contribution to spring energy may be ignored, so that the J-integral result (16) becomes

$$\frac{(1-\nu^2)K^2}{E} = \frac{(1-\nu^2)K_m^2}{E} + 2\sigma_Y v_P \qquad (24)$$

and the toughening ratio is

$$\lambda = \left[1 + \frac{2E\sigma_Y v_P}{K_m^2(1-\nu^2)}\right]^{1/2} \qquad (25)$$

The result for λ in terms of bridge length follows from (11) with $\sigma(x)=\sigma_Y$; thus

$$\lambda = 1 + 2\sqrt{\frac{2}{\pi}}\frac{\sigma_Y\sqrt{L}}{K_m} \qquad (26)$$

PARTICULATE TOUGHENING

Particle-pinned-crack model

For simplicity, we will assume spherical particles, and suppose that the faces of an advancing plane crack are pinned by the particles at their equators (Fig. 1). Consistency with this assumption would require that the matrix area on the bridged zone be reduced by a fraction that exceeds the volume concentration c of particles. However, again for simplicity, we will suppose that the matrix-area concentration of each crack face retains the value (1- c) that corresponds to an arbitrary plane cross-section of the composite material. To invoke the bridging-spring model of Fig. 2, we will identify the spring stress $\sigma(x)$ with smeared-out particle stresses $c\sigma_p(x)$, where $\sigma_p(x)$ is the average particle stress at x — that is, the average over all particles in the thickness direction, normal to the plane of Fig. 1. Next, we have to get an estimate for the effective spring constant k.

Effective spring constant

Consider first two elastic half-spaces, bridged by a *single* isolated elastic particle, that are pulled apart by remote tensile forces that produce an average tensile stress σ_p in its equatorial cross-section. If we neglect the difference between the particle and matrix moduli, the remote displacement of each face (Fig. 6a) is given by the classical smooth-punch result

$$v = \frac{\pi a(1-\nu_m^2)\sigma_p}{2E_m} \tag{27}$$

where E_m and ν_m are the Young's modulus and Poisson's ratio of the matrix, and a is the particle radius. This is the average crack-face displacement for the limit $c \to 0$. For arbitrary c we will write

$$v_{ave} = \beta(c)\frac{\pi a(1-\nu_m^2)\sigma_p}{2E_m} \tag{28}$$

and estimate β on the basis of the circumferentially cracked cylinder shown in Fig. 6b, with outer radius b chosen to satisfy $(a/b)^2 = c$ in order to meet the assumed crack-face area ratio. (Here v_{ave} is defined as the displacement averaged over the full area πb^2 of the cylinder.) For this configuration, Tada

et al. (1985) supply the following approximate relations for the crack stress-intensity factor:

$$K_I = \sigma \frac{\sqrt{\pi a(1 - a/b)}}{2(a/b)^2} H(a/b) \tag{29a}$$

$$H(a/b) = 1 + \frac{1}{2}(a/b) + \frac{3}{8}(a/b)^2 - .363(a/b)^3 + .731(a/b)^4 \tag{29b}$$

where the applied stress is $\sigma = (a/b)^2\sigma_p$. The energy released by cutting the crack into the cylinder in the presence of constant σ is given by the integral

$$2\pi \int_a^b \frac{K_I^2(1-\nu_m^2)}{E_m} a'da' \tag{30}$$

and this may be equated to $\pi b^2 \sigma v_{ave}$. The resulting expression for v_{ave} may then be compared with Eq. (28) to yield the formula

$$\beta = \sqrt{c} \int_{\sqrt{c}}^1 (1-\rho)\left[\frac{H(\rho)}{\rho}\right]^2 d\rho \tag{31}$$

Finally, substituting v_{ave} into the defining relation (2) for k, we get

$$k = \left(\frac{2c}{\pi\beta a}\right)\left(\frac{E_m}{1-\nu_m^2}\right)\left(\frac{1-\nu^2}{E}\right) \tag{32}$$

Here E and ν are the effective elastic constants of the <u>composite</u> material consisting of the ceramic matrix containing a randomly distributed concentration c of particles.

The function $\beta(c)$ defined by Eq. (31) is shown by the solid curve in Fig. 7. The dashed curve shows the approximation provided by the empirical formula

$$\beta \approx (1-c)(1-\sqrt{c}) \tag{33}$$

Since this estimate for β is explicit and simple, we will use it henceforth.

Toughening ratio

We can now rewrite the J-integral results (4) and (5) to make them applicable to a ceramic reinforced by elastic particles. The left-hand side of (4), which comes from the far field, stays the same, but now E and ν refer to the effective properties of the composite. The first term on the right came from the energy-release rate at the crack edge, and so we should change E and ν to E_m and ν_m because the crack edge is advancing only into matrix material. We also multiply this term by (1-c) to take into account the fact that the bridging particles reduce the length of the advancing crack front by the factor c. This gives

$$\frac{K^2(1-\nu^2)}{E} = \frac{K_m^2(1-\nu_m^2)(1-c)}{E_m} + \frac{(1-\nu^2)\sigma^2(L)}{kE} \tag{34}$$

Finally, we use Eqs. (32) and (33) to substitute for k in the last term, and set $\sigma(L) = \sigma_Y = cS$, where S, the particle strength, is the magnitude of the particle stress σ_p at failure. The result is

$$\frac{K^2(1-\nu^2)}{E} = \frac{K_m^2(1-\nu_m^2)(1-c)}{E_m} + \frac{\pi}{2}\frac{S^2ac(1-c)(1-\sqrt{c})(1-\nu_m^2)}{E_m} \tag{35}$$

(Here we should interpret K_m as the root-mean-square value of the stress-intensity factor in the ceramic along the crack front.) Then, for the case of particles that break elastically, we get the *modified* toughening ratio

$$\Lambda \equiv \frac{K/K_m}{\sqrt{\omega(1-c)}} = \left\{1+\frac{\pi}{2}\frac{S^2ac(1-\sqrt{c})}{K_m^2}\right\}^{1/2} \tag{36}$$

where

$$\omega = \frac{E(1-\nu_m^2)}{E_m(1-\nu^2)} \tag{37}$$

Similarly, the J-integral results (16) and (17) for elastic-ideally plastic springs can be adapted to apply to ceramics containing ductile particles that undergo plastic flow before they fail. For the configuration of Fig. 6 the

connection between average particle stress σ_p and v_{ave} up to failure is now presumed to be like that shown by the solid curve in Fig. 8. We idealize this function, replacing it with the elastic-plastic relation given by the dotted lines, choosing S as the peak particle stress, and picking v_P so as to make the areas under the two curves the same. (Unfortunately, little information is available concerning actual σ_p- v_{ave} relations, so the idealization is only conceptual.) Then the elastic-plastic counterpart of (35) is found by multiplying its last term by the factor $(1+2v_P/v_Y)$, and the modified toughening ratio becomes

$$\Lambda \equiv \frac{K/K_m}{\sqrt{\omega(1-c)}} = \left\{1+\frac{\pi}{2}\frac{S^2 ac(1-\sqrt{c})}{K_m^2}\left(1+2\frac{v_P}{v_Y}\right)\right\}^{1/2} \tag{38}$$

For a given strength S, the effect of pre-failure ductility is clearly substantial; however, the lowered particle constraint associated with increasing v_P/v_Y may be expected to lower S.

Finally, the toughening for the limiting case $v_P/v_Y \to \infty$ may be calculated by modifying the J-integral result (24) for rigid-plastic springs. Thus

$$\frac{K^2(1-\nu^2)}{E} = \frac{K_m^2(1-\nu_m^2)(1-c)}{E_m} + 2cSv_P \tag{39}$$

and this gives

$$\Lambda \equiv \frac{K/K_m}{\sqrt{\omega(1-c)}} = \left[1+\frac{2c}{1-c}\frac{E_m S v_P}{K_m^2(1-\nu_m^2)}\right]^{1/2} \tag{40}$$

Toughening vs. bridge length: matrix crack-growth resistance

With λ replaced by the modified toughening ratio Λ defined above, and the use of Eqs. (32) and(33) to evaluate k, the results of Fig. 4 for toughening versus bridge length may be applied to particle-reinforced ceramics. For convenience, the curves of Fig. 4 are rescaled in Fig. 9 to show Λ versus $(\pi^2\alpha/8)$, which now equals

$$\rho \equiv \frac{c}{(1-c)(1-\sqrt{c})}\frac{L}{\omega a} \tag{41}$$

(The symbols in Fig. 9 represent experimental data to be discussed later.) Besides the connection these curves give between L/a at fracture and the toughening ratio, they have another interpretation as *resistance curves* associated with matrix crack growth that is *not* accompanied by particle fracture. Suppose a pre-existent crack in the composite is subjected to a gradually increasing far-field K and think of Λ as the current value of the ordinate of Fig. 9 during this loading process. At $\Lambda=1$ the crack will begin to advance into the matrix, but particles will remain intact as long as Λ is below its critical value for *composite* fracture. If we now let L denote the amount of bridged matrix crack growth that occurs before failure, the relation between K and L is provided by the curves of Fig. 9.

For $v_P/v_Y \to \infty$, the relation between toughening and bridge length is produced by changing Eq. (26) to read

$$\Lambda = 1 + 2\sqrt{\frac{2}{\pi}}\,\frac{cS\sqrt{L}}{K_m} \tag{42}$$

Toughening vs. concentration; bridge length vs. concentration

The toughening ratio K/K_m generally starts out as an increasing function of c, but its rate of increase may drop substantially as c goes up. For the case of very ductile particles, this is illustrated in Fig. 10a when the ratio of matrix and particle moduli is $E_m/E_p=5$. Here Eq.(40) has been used to calculate K/K_m versus c, for several values of $Z=S\sqrt{L_o}/K_m$, where

$$L_0 = \frac{\pi}{8}\left[\frac{E_m v_P}{K_m(1-\nu_m^2)}\right]^2 \tag{43}$$

The parameter ω defined by Eq.(37) was calculated as a function of c on the basis of the self-consistent method (Hill 1965; Budiansky 1965).

Similar results may generally be expected for finite v_P/v_Y. However, for a sufficiently small value of v_P/v_Y, K/K_m may reach a maximum at a moderate value of c. (For the limiting case of elastic particles, with $E_m/E_p>1$, Eq.(36) implies a maximum value of K/K_m at $c < .29$)

It follows from Eqs.(40) and (42) that for very ductile particles

$$\frac{L}{L_0} = \frac{4}{(\Lambda+1)^2}\left(\frac{\omega}{1-c}\right) \tag{44}$$

Since, generally, $\omega<(1-c)$ for $E_m/E_p>1$, the critical bridge length is a decreasing function of c, as illustrated in Fig. 10b for $v_P/v_Y \to \infty$. Furthermore, it can be shown that L is a decreasing function of c for *all* v_P/v_Y.

EXPERIMENTAL INFORMATION

Some available experimental measurements of bridge lengths as well as toughening in several composite systems will be examined in the light of the present analysis. Krstic et al. (1981) tested a model system consisting of glass reinforced by aluminum particles, and Sigl et al. (1987) report results of studies of Al_2O_3/Al and WC/Co. The toughness K and the bridging zone size L were measured by placing cracks into the composite, imposing external loads, and observing the stretched metal ligaments between the surfaces at final fracture. For each composite, the data to be discussed are for a 20% volume concentration of particles.

Table II lists the measured values of K, L, and the average particle radius a; bulk elastic constants of matrix (E_m, ν_m) and particle (E_p, ν_p); elastic constants of the composites (E, ν), calculated self-consistently; matrix toughness K_m; and the estimated uniaxial yield strength σ_o of bulk particle material. Based on these data, the points plotted in Fig. 9 show the corresponding values of Λ and ρ. The effective values of v_P/v_Y that may be inferred are $v_P/v_Y \approx 41$ for the glass/Al system, ≈ 68 for Al_2O_3/Al, and ≈ 12 for WC/Co.

These inferred values of v_P/v_Y may be used in conjunction with the toughening formula (38) to back-figure effective particle strengths S. For the particles in glass/Al, we find $S \approx 250$ MPa, which gives $S/\sigma_o \approx 3.6$. But a much higher strength, $S \approx 1500$ MPa, is calculated for the considerably smaller aluminum particles in the Al_2O_3/Al system. This gives $S/\sigma_o \approx 22$, and the same surprisingly high ratio is obtained for the small cobalt particles in WC/Co, for which Eq. (38) gives $S \approx 10$ GPa.

For Al_2O_3/Al, the rigid-plastic model seems appropriate, and, indeed, using Eq.(42) to estimate S provides a result only slightly lower than that

given by the elastic-plastic model. Finally, we remark that the use of this calculated value of S ≈ 1500 MPa in Eq.(40) to compute the plastic particle stretch gives $v_P \approx .3\ \mu m$. Sigl et al. (1987) measured stretches ≈ 1μm in severely necked-down particles before fracture.

CONCLUDING REMARKS

Our theoretical study of particulate toughening displays the effects of particulate strength, deformation, and size on toughening. In the case of elastic particles, Eq.(36) shows that for a given particle strength, toughening is an increasing function of particle size. The same is true for plastically deforming particles (Eqs.(38,40)) if we assume that both V_P and V_Y are proportional to particle radius. Large plastic deformation of the bridging particles before fracture can have a substantial toughening effect, and high particle strength is obviously desirable. But the actual strength and ductility of a bridging particle are, at this time, difficult parameters to assess, since they may well be greatly influenced by load and shape asymmetries, as well as by interface sliding, all of which tend to reduce constraint on the particle, promote plastic flow, and lower its strength.

Confrontation of experimental data on metal-reinforced ceramics with the predictions of the present theory seems to imply suspiciously high particle strengths. If such high strengths are not confirmed, toughening mechanisms in addition to crack bridging may be operative in particulate-reinforced ceramics.

ACKNOWLEDGEMENTS

This work was initiated by the DARPA Materials Research Council under the auspices of the University of Michigan, and was continued with support from the National Science Foundation (Grant MSM-84-16392), the Office of Naval Research (Contract N00014-84-K-0510), DARPA University Research Initiative (Subagreement P.O. #VB38639-0 with the University of California, Santa Barbara, ONR Prime Contract N00014-86-K-0753), and the Division of Applied Sciences, Harvard University.

REFERENCES

Budiansky, B., 1965, "On the Elastic Moduli of Some Heterogeneous Materials", J. Mech Phys. Solids, 13, pp. 223-227.

Budiansky, B., 1986, "Micromechanics II", Proceedings of the Tenth U. S. National Congress of Applied Mechanics", Austin, Texas, June 16-20, 1986.

Hill, R., 1965, "A Self-Consistent Mechanics of Composite Materials", J. Mech. Phys. Solids, 13, pp. 213-222.

Krstic, V. D., Nicholson, P. S. and Hoagland, R. G., 1981, "Toughening of Glasses by Metallic Particles", J. Am. Ceram. Soc., 64, pp. 499-504.

Krstic, V. D., 1983, "On the Fracture of Brittle-Matrix/Ductile-Particle Composites", Phil. Mag. A, 48, No. 5, pp. 695-708.

Rice, J. R., 1968, "A Path Independent Integral and the Approximate Analysis of Strain Concentration by Notches and Cracks", Jour. of Applied Mechanics, 35, pp. 379-386.

Rose, L. R. F., 1986, "Crack Reinforcement by Distributed Springs", J. Mech. Phys. Solids (in press).

Sigl, L., Mataga, P., Dalgleish, B. J., McMeeking, R. M., and Evans, A. G., "On the Toughness of Brittle Materials Reinforced with a Ductile Phase", to be published.

Tada, H., Paris, P.C., and Irwin, G. R., 1985, "The Stress Analysis of Cracks Handbook", Del Research, St. Louis, MO.

APPENDIX A
Integral-Equation Solutions

Elastic springs

A convenient set-up for solving the integral equation (8) is obtained by differentiation, which gives

$$g'(s) + \frac{1}{2}\int_0^{\alpha} \sqrt{\frac{t}{s}}\,\frac{g(t)}{t-s}\,dt = \frac{1}{2\sqrt{s}} \tag{A1}$$

To satisfy the original integral equation (8), we have to enforce it at just one point, say $\alpha=s$, in addition to satisfying (A1) for s in $(0,\alpha)$. Note that (8), (12), and (A1) imply that

$$g(s) \sim \frac{\sqrt{s}}{\lambda} \qquad \text{for } s\to 0 \tag{A2}$$

If we now let

$$g(s) = \frac{H(s)}{\sqrt{s}} \tag{A3}$$

then (A1) reduces to

$$2sH'(s) - H(s) + s\int_0^{\alpha} \frac{H(t)}{t-s}\,dt = s \tag{A4}$$

A neat way to proceed is to write

$$H(s) = A(s/\alpha) + f(s) \tag{A5}$$

where $A = \sqrt{\alpha}g(\alpha)$, and $f(0) = f(\alpha) = 0$. Then

$$A\left[\left(\frac{1}{\alpha}+1\right)s + \frac{s^2}{\alpha}\log\left(\frac{\alpha-s}{s}\right)\right] + 2sf'(s) - f(s) + s\int_0^{\alpha}\frac{f(t)dt}{t-s} = s \tag{A6}$$

and with

$$s = \frac{\alpha}{2}(1-\cos\theta) \tag{A7}$$

the Fourier-series expansion

$$f = \sum_{n=1}^{N} a_n \sin(n\theta) \tag{A8}$$

is appropriate. Since

$$\int_0^{\alpha} \frac{f(t)dt}{t-s} = \pi \sum_{n=1}^{N} a_n \cos(n\theta) \tag{A9}$$

Eq.(A8) becomes

$$A\left[\left(\frac{1+\alpha}{2}\right)(1-\cos\theta) + \frac{\alpha}{4}(1-\cos\theta)^2 \log\left(\frac{1+\cos\theta}{1-\cos\theta}\right)\right] + 2\left(\frac{1-\cos\theta}{\sin\theta}\right)\sum_{n=1}^{N} n a_n \cos n\theta$$

$$-\sum_{n=1}^{N} n a_n \sin n\theta + \frac{\pi\alpha(1-\cos\theta)}{2} \sum_{n=1}^{N} a_n \cos n\theta = \frac{\alpha}{2}(1-\cos\theta) \tag{A10}$$

If we now multiply (A10) by $\sin(m\theta)$ and integrate over $(0,\alpha)$ we get

$$C_m A - \frac{\pi}{2}\sum_{n=1}^{N} D_{mn}\, a_n = \alpha E_m \qquad (m=1,2,\ldots) \tag{A11}$$

where

$$C_m = (1+\alpha)E_m + \frac{\alpha}{4}T_m$$

$$F_m = \frac{1}{m} \qquad (m \text{ odd})$$

$$= -\frac{m}{m^2-1} \qquad (m \text{ even})$$

$$D_{mn} = 2\alpha P_{mn} \qquad (m < n)$$

$$= 1 + 2n + 2\alpha P_{mn} \qquad (m=n)$$

$$= 4n(-1)^{m+n} + 2\alpha P_{mn} \qquad (m > n)$$

$$P_{mn} = -\frac{m}{m^2 - n^2} \qquad (m+n \text{ odd})$$

$$= \frac{m(m^2 - n^2 - 1)}{(m^2 - n^2 - 1)^2 - 4n^2} \qquad (m+n \text{ even})$$

and

$$T_m = \int_0^{\pi} (1-\cos\theta)^2 \log\left(\frac{1+\cos\theta}{1-\cos\theta}\right) \sin(m\theta)\, d\theta$$

was evaluated numerically. The substitution of (A5) into the undifferentiated integral equation (8), and its assertion at the point $s=\alpha$ leads to

$$P_0 A + \sum_{n=1}^{N} P_n a_n = 1 \qquad (A12)$$

where

$$P_0 = \left[\frac{1}{\alpha} + \frac{1 + 2\log 2}{3}\right]$$

and

$$P_n = \int_0^{\pi} \left(\cos\frac{\theta}{2}\right) \log\left(\frac{1+\sin\frac{\theta}{2}}{\cos\frac{\theta}{2}}\right) \sin(n\theta)\, d\theta \qquad (n \geq 1)$$

was evaluated numerically.

Equations (A11) and (A12) constitute N+1 linear equations for A and a_n (n=1,2,3,...N). The formula (12) for λ works out neatly to

$$\lambda = \left[1 - A - \pi \sum_{n=1}^{N} a_n\right]^{-1} \qquad (A13)$$

and the independent result (10) that can be used to check this is just

$$\lambda = [1 - 2A^2/\alpha]^{-1/2} \qquad (A14)$$

An alternative procedure that gave slightly more accurate results for a given number of simultaneous equations was provided by the use of the substitution

$$H(s) = A(s/\alpha)^2 + f(s) \tag{A15}$$

in place of (A5). The first term in (A6) then changes to

$$A\left[\frac{s}{2} + \left(\frac{1}{\alpha} + \frac{3}{\alpha^2}\right)s^2 + \frac{s^3}{\alpha^2}\log\left(\frac{\alpha - s}{s}\right)\right]$$

and the system of equations (A11) and (A12) for A and a_n (n=1,2,...N) remains valid, except that C_m and P_0 change to

$$C_m' = \frac{(3+\alpha)H_m}{4} + \frac{\alpha}{2}F_m + \frac{\alpha}{8}W_m$$

and

$$P_0' = \frac{1}{\alpha} + \frac{3+4\log 2}{10}$$

where

$$H_m = \frac{4(m^2-3)}{m(m^2-4)} \qquad (m \text{ odd})$$

$$= -\frac{4m}{m^2-1} \qquad (m \text{ even})$$

and

$$W_m = \int_0^{\pi} (1-\cos\theta)^3 \log\left(\frac{1+\cos\theta}{1-\cos\theta}\right)\sin(m\theta)\,d\theta$$

is evaluated numerically. The formula (A13) changes to

$$\lambda = \left[1 - \frac{A}{2} - \pi\sum_{n=1}^{N} a_n\right]^{-1} \tag{A16}$$

but (A14) stays the same. For values of α up to 30, solutions based on (A16) and (A17) with N=60 were judged to be quite accurate, because they gave values for λ according to the independent formulas (A16) and (A14) that were in excellent agreement with each other (1% discrepancy at α=30, and less at lower α's). The final results shown for λ in Table I were obtained by extrapolation to N=∞.

Elastic-plastic springs

To solve (19) for g(s) in the range $(0,\alpha_Y)$, we differentiate, as before, and again use the substitution (A3) to get

$$2sH'(s) - H(s) + s\int_0^{\alpha_Y} \frac{H(t)}{t-s}\,dt + g_Y\int_{\alpha_Y}^{\alpha} \frac{\sqrt{t}}{t-s} = s \qquad \text{(A17)}$$

Now with

$$H(s) = A(s/\alpha_Y)^2 + f(s) \qquad \text{(A18)}$$

and

$$s = \frac{\alpha_Y}{2}(1-\cos\theta) \qquad \text{(A19)}$$

we can retain the Fourier expansion (A8) for f (this time for s in $(0, \alpha_Y)$. Once again we get equations (A11) and (A12), with revised formulas for C_m and P_0 given by

$$C_m'' = C_m' + 2\left(\sqrt{\alpha\alpha_Y} - \alpha_Y\right)F_m - \alpha_Y U_m$$

$$P_0 = P_0' + \frac{1}{2}\left(\frac{\alpha}{\alpha_Y} - 1\right)\log\frac{1+\sqrt{\alpha_Y/\alpha}}{1-\sqrt{\alpha_Y/\alpha}} + \sqrt{\frac{\alpha}{\alpha_Y}} - 1$$

where

$$U_m = \int_0^{\pi} \log\frac{\left(1+\sqrt{\alpha_Y/\alpha}\,\sin\frac{\theta}{2}\right)\left(1-\sin\frac{\theta}{2}\right)}{\left(1-\sqrt{\alpha_Y/\alpha}\,\sin\frac{\theta}{2}\right)\left(1+\sin\frac{\theta}{2}\right)}\sin^3\frac{\theta}{2}\sin(m\theta)\,d\theta$$

The expression (21) for v_P/v_Y may be evaluated as

$$v_p/v_Y = -1 + \frac{\sqrt{\alpha\alpha_Y}}{A} - \frac{\alpha_Y}{5}\left[\log\frac{1+\sqrt{\alpha_Y/\alpha}}{1-\sqrt{\alpha_Y/\alpha}} + \left(\frac{\alpha}{\alpha_Y}\right)^{5/2}\log(1-\alpha_Y/\alpha) + \frac{1}{2}\sqrt{\alpha/\alpha_Y} + \left(\frac{\alpha}{\alpha_Y}\right)^{3/2}\right]$$

$$-\alpha\left[1 - \sqrt{\alpha_Y/\alpha} + \frac{1}{2}(1-\alpha_Y/\alpha)\log\frac{1+\sqrt{\alpha_Y/\alpha}}{1-\sqrt{\alpha_Y/\alpha}}\right] - \frac{\alpha_Y}{2A}\sum_{n=1}^{N} Q_n a_n$$

where

$$Q_n = \int_0^{\pi} \cos\frac{\theta}{2}\sin(n\theta)\log\frac{1+\sqrt{\alpha_Y/\alpha}\,\sin\frac{\theta}{2}}{1-\sqrt{\alpha_Y/\alpha}\,\sin\frac{\theta}{2}}\,d\theta$$

and the formula (23) gives

$$\lambda = \left[1 - \frac{A}{2}\left(4\sqrt{\alpha/\alpha_Y} - 3\right) - \pi\sum_{n=1}^{N} a_n\right]^{-1} \qquad \text{(A20)}$$

APPENDIX B

Consistency of Formulas for Toughening Ratio

We want to show that if g(s) satisfies the integral equation (8), then the formulas (10) and (12) give the same answer for λ. It will suffice to prove that

$$\left[1-\int_0^\alpha \frac{g(s)ds}{\sqrt{s}}\right]^2 + 2g^2(\alpha) = 1 \tag{B1}$$

if g(0) = 0, and Eq.(A1) is satisfied. From (A1)

$$g(s)g'(s) + \frac{1}{2}\int_0^\alpha \sqrt{\frac{t}{s}}\frac{g(s)g(t)}{t-s}dt = \frac{g(s)}{2\sqrt{s}} \tag{B2}$$

and integration gives

$$\frac{1}{2}g^2(\alpha) + \frac{1}{2}\int_0^\alpha\int_0^\alpha \sqrt{\frac{t}{s}}\frac{g(s)g(t)}{t-s}dtds = \frac{1}{2}\int_0^\alpha \frac{g(s)}{\sqrt{s}}ds \tag{B3}$$

To show that (B3) implies (B1), we just have to verify that

$$\left[\int_0^\alpha \frac{g(s)ds}{\sqrt{s}}\right]^2 = 2\int_0^\alpha\int_0^\alpha \sqrt{\frac{t}{s}}\frac{g(s)g(t)}{t-s}dtds \tag{B4}$$

But if the integrals exist this is an identity, because

$$\int_0^\alpha\int_0^\alpha\left[\sqrt{\frac{t}{s}}-\sqrt{\frac{s}{t}}\right]\frac{g(s)g(t)}{t-s}dsdt \equiv \int_0^\alpha\int_0^\alpha \frac{g(s)g(t)}{\sqrt{st}}dsdt = \left[\int_0^\alpha \frac{g(s)}{\sqrt{s}}ds\right]^2$$

and

$$\int_0^\alpha\int_0^\alpha\left[\sqrt{\frac{t}{s}}+\sqrt{\frac{s}{t}}\right]\frac{g(s)g(t)}{t-s}dsdt = 0$$

APPENDIX C

Elastic Springs, $\alpha \to \infty$

If we let $\xi = \pi(\alpha - s)/2$ in Eq.(A1), and then let $\alpha \to \infty$, we get

$$g'(\xi) - \frac{1}{\pi}\int_0^\infty \frac{g(\eta)}{\xi-\eta}d\eta = 0 \qquad (\xi \geq 0) \tag{C1}$$

which has to be solved subject to the condition

$$g \approx \frac{1}{\sqrt{2\pi\xi}} \qquad \text{for } \xi \to \infty \tag{C2}$$

that is consistent with the far-field stresses (1). Let $f(\xi)$ denote the right hand side of (C1) for $\xi < 0$, and say $g(\xi) = 0$ for $\xi < 0$. Then the Fourier transforms

$$\bar{g}(\omega) \equiv \int_{-\infty}^{\infty} g(\xi)e^{i\omega\xi}d\xi \qquad \bar{f}(\omega) \equiv \int_{-\infty}^{\infty} f(\xi)e^{i\omega\xi}d\xi$$

satisfy

$$\frac{\omega}{|\omega|}(1+|\omega|)\bar{g}^+ = i[\bar{f}^- + g(0)] \tag{C3}$$

Here the + and - superscripts denote analyticity in the upper and lower half ω-planes, respectively. Now split $(1+|\omega|)$ into the quotient Q^+/Q^- by writing

$$\frac{(Q^+)'}{Q^+} - \frac{(Q^-)'}{Q^-} = \frac{\omega/|\omega|}{1+|\omega|}$$

from which we find

$$\frac{(Q^+)'}{Q^+} = \frac{1}{2\pi i}\int_{-\infty}^{\infty} \frac{x/|x|}{(1+|x|)(x-\omega)}dx$$

$$= \frac{1}{2(1+\omega)} - \frac{i \log \omega}{\pi(\omega^2-1)} \qquad (\mathrm{Im}(\omega) > 0)$$

Integration gives

$$Q^+ = (\mathrm{const})\sqrt{1+\omega}\,\exp\left(-\frac{i}{\pi}\int_0^{\omega} \frac{\log z\, dz}{z^2-1}\right)$$

Since $\omega/|\omega|$ splits into $(\sqrt{\omega})^+/(\sqrt{\omega})^-$, Eq.(C3) implies that

$$(\sqrt{\omega})^+ Q^+ \bar{g}^+ = i[\bar{f} + g(0)](\sqrt{\omega})^- Q^-$$

is an entire function of ω, and the right choice will turn out to be a constant. Thus

$$\bar{g}(\omega) = \frac{C}{\sqrt{\omega(1+\omega)}}\exp\left[\frac{i}{\pi}\int_0^{\omega} \frac{\log z\, dz}{z^2-1}\right] \qquad (C4)$$

the only singularity of which is a branch point at the origin. Evaluating the inversion integral

$$g(\xi) = \frac{1}{2\pi i}\int_{-\infty}^{\infty} \bar{g}(\omega)\exp(-i\omega\xi)\, d\omega$$

via integration around the branch cut from 0 to $-i\infty$ gives

$$g(\xi) = Ce^{-\pi i/4}\int_0^{\infty} \frac{\exp\left(-t\xi - \frac{1}{\pi}\int_0^t \frac{\log \tau\, d\tau}{1+\tau^2}\right)}{\sqrt{t}\,(1+t^2)^{3/4}}\, dt \qquad (C5)$$

For large ξ this can be evaluated asymptotically via Watson's lemma, and matching the behavior for $\xi \to \infty$ to that given by Eq.(C2) gives

$$g(\xi) \approx \frac{1}{\sqrt{2\pi\xi}} - \frac{1}{(2\pi\xi)^{3/2}}[\psi(3/2) - 1 - \log \xi] + \cdots$$

$$(\psi[z] \equiv \Gamma'[z]/\Gamma[z])$$

with C= (1+i)/2. To get an expansion of $g(\xi)$ for ξ small, use (C4) to write the Laplace transform

$$\hat{g}(s) \equiv \int_0^\infty e^{-s\xi} g(\xi)\, d\xi = \bar{g}(is) \qquad (s>0)$$

as

$$\hat{g}(s) = (2s)^{-1/2}(1+s^2)^{-1/4} \exp\left[\frac{1}{\pi}\int_0^s \frac{\log \rho\, d\rho}{1+\rho^2}\right]$$

Expanding this for large s gives

$$\hat{g}(s) \approx \frac{1}{\sqrt{2}}\left[\frac{1}{s} - \frac{1}{\pi}\left(\frac{\log s + 1}{s^2}\right) + \cdots\right]$$

and from term-by-term inversion we get

$$g(\xi) \approx \frac{1}{\sqrt{2}} - \frac{\xi}{\pi\sqrt{2}}[1 - \gamma - \log \xi] + \ldots$$

$$\gamma = -\Gamma'(1) \approx .57722 \ldots$$

Finally, with $Ce^{-\pi i/4} = 1/\sqrt{2}$, Eq.(C5) was used to evaluate $g(\xi)$ for intermediate values of ξ via numerical integration.

α	.25	.5	1	2	5	10	15	20	25	30
λ	1.244	1.478	1.91	2.68	4.44	6.54	8.15	9.51	10.70	11.76

TABLE I : λ vs. α for elastic springs

System	K (MPa$\sqrt{m}$)	L (μm)	a (μm)	E_m (GPa)	ν_m	E_p (GPa)	ν_p	E (GPa)	ν	K_m (MPa$\sqrt{m}$)	σ_0 (MPa)
glass/Al (c = .2)	6.5	6000	55	68.9	.20	68.9	.33	69.2	.23	.8	70
Al_2O_3/Al (c = .2)	8.4	160	2	420	.20	70	.33	308	.22	3	70
WC/Co (c = .2)	16	10	.75	710	.21	210	.31	566	.22	8	450

TABLE II : Experimental data and material properties

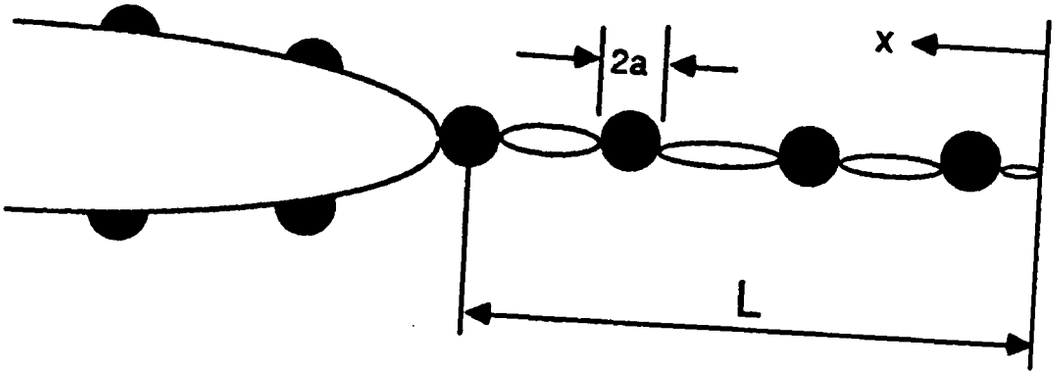

Fig. 1. Bridged crack.

Far-field: $\sigma_{\alpha\beta} \approx \frac{K f_{\alpha\beta}(\theta)}{\sqrt{2\pi r}}$

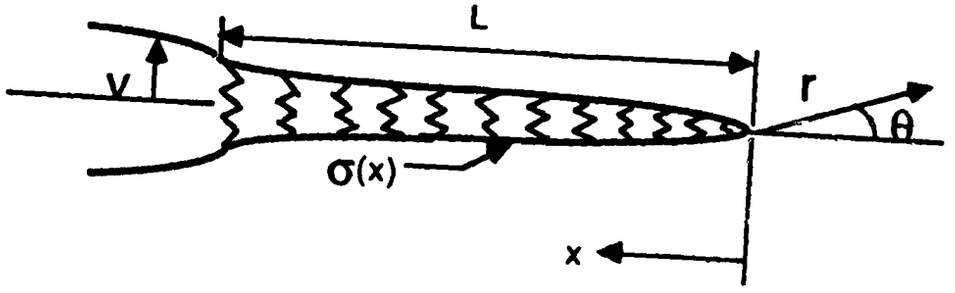

Fig. 2. Bridging-spring model.

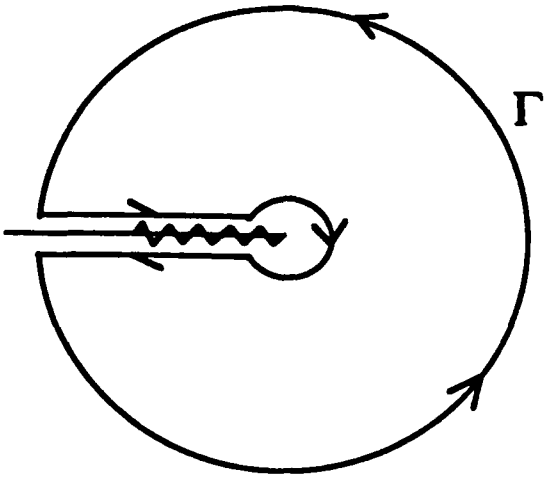

Fig. 3. J-integral path.

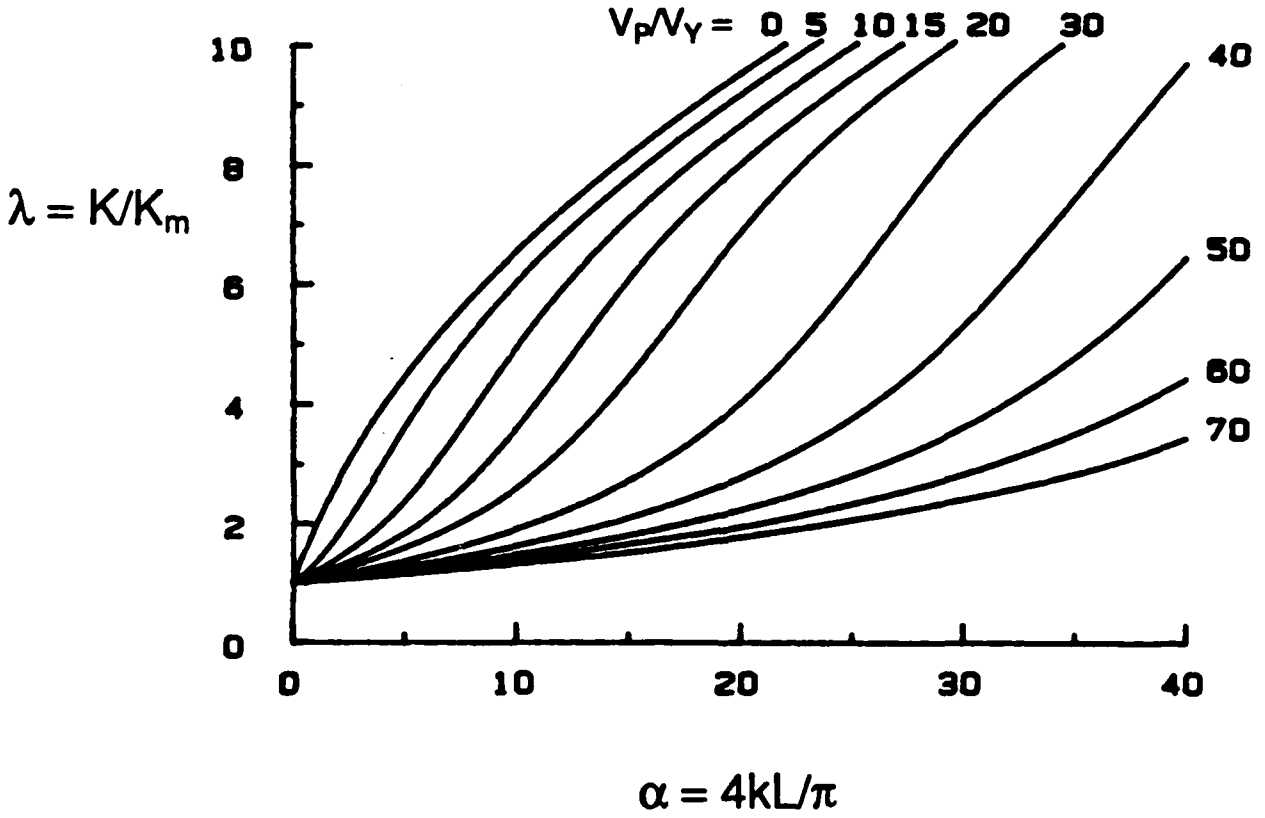

Fig. 4. Bridging-spring model: toughening vs. bridge length

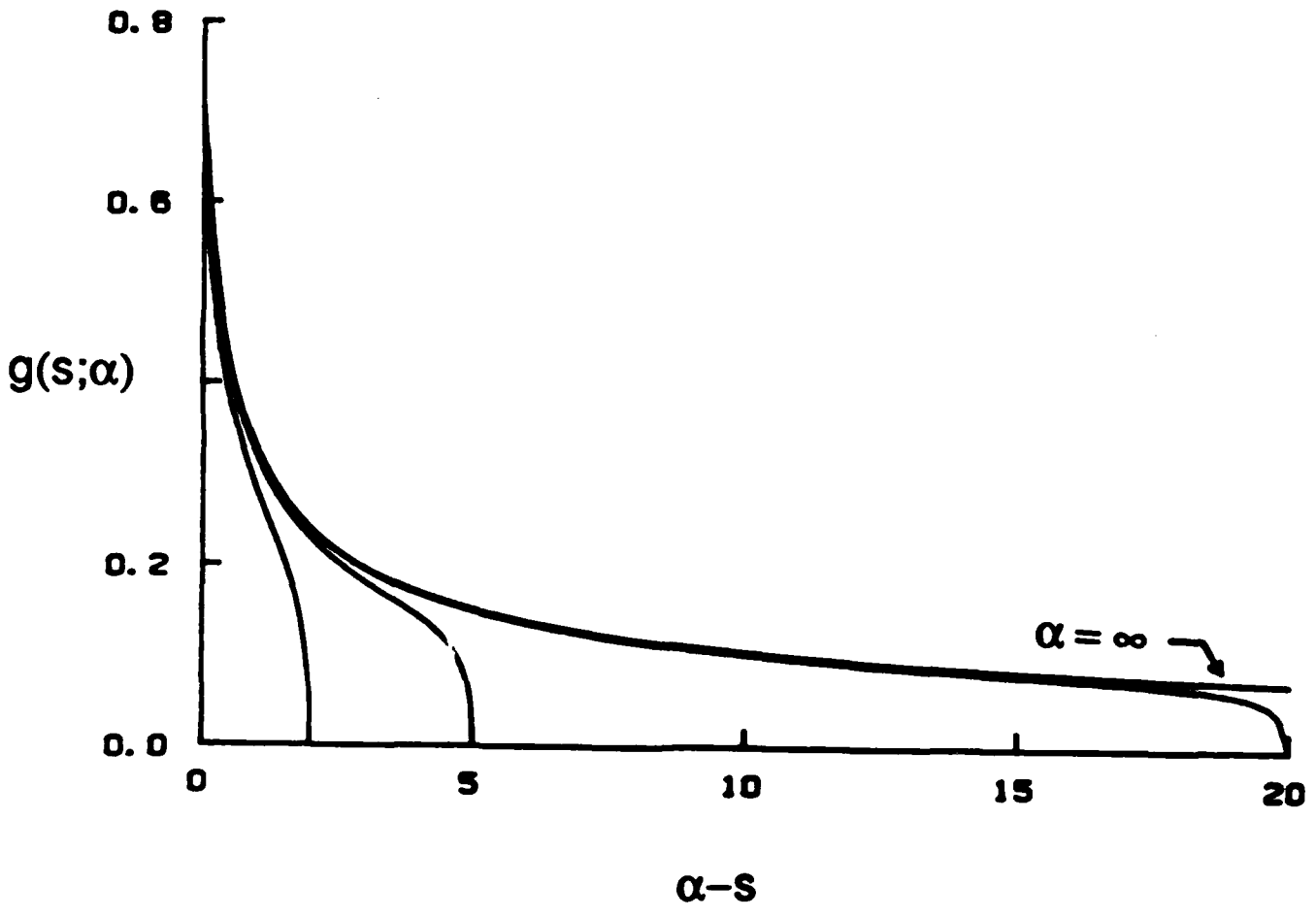

Fig. 5. Elastic springs: non-dimensional spring-stress distribution

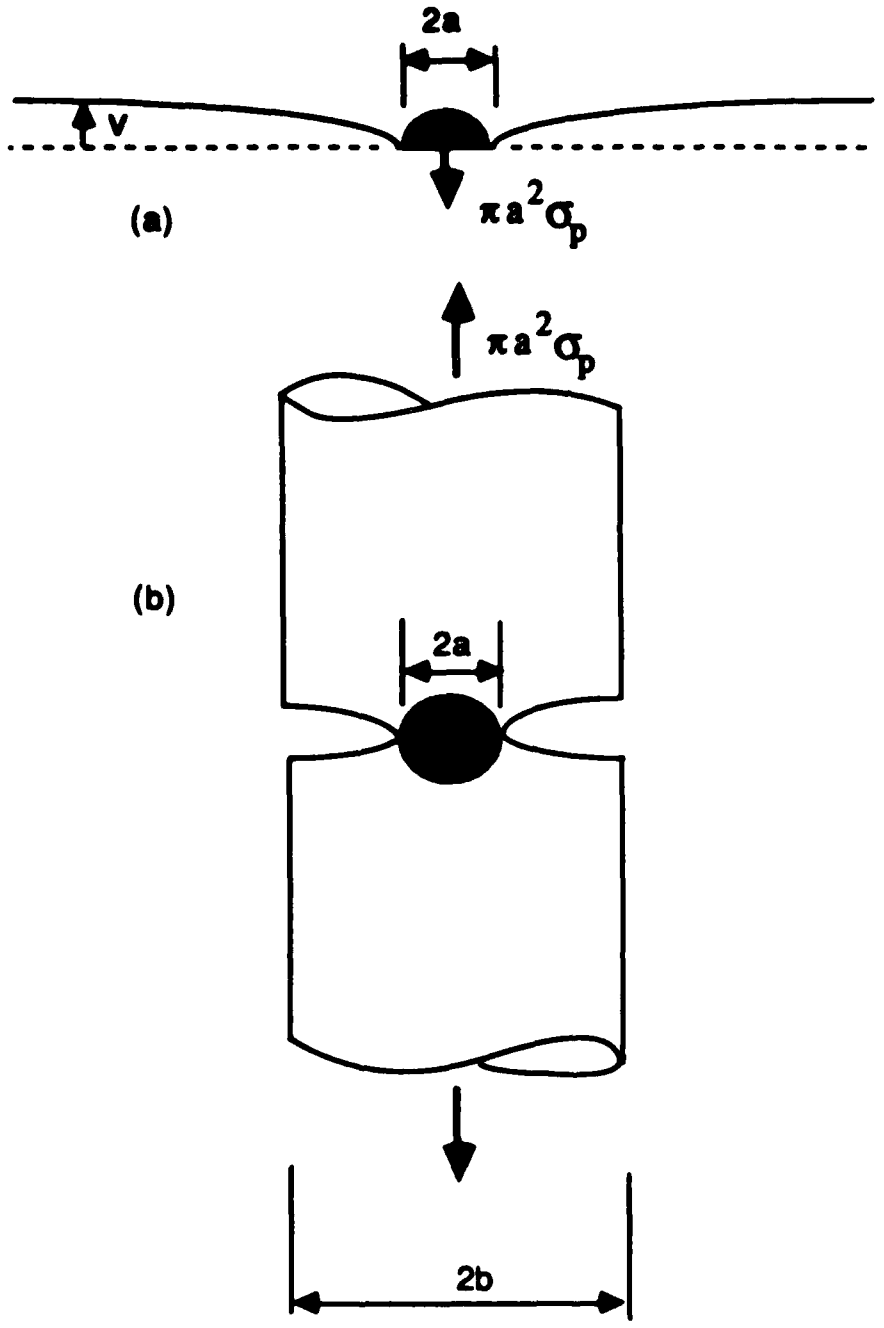

Fig. 6. Crack opening: (a) c --> 0 (b) $c = (a/b)^2$

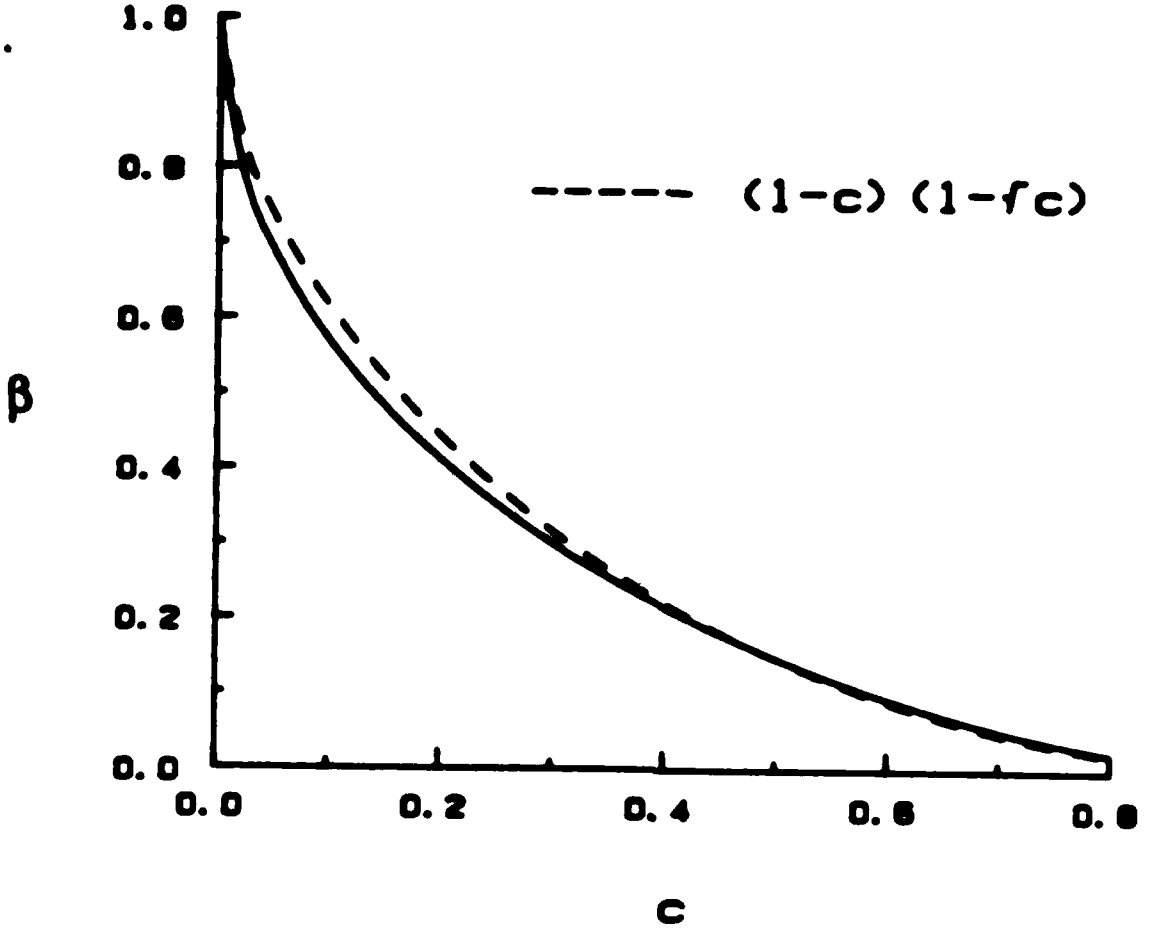

Fig. 7. Average-displacement factor

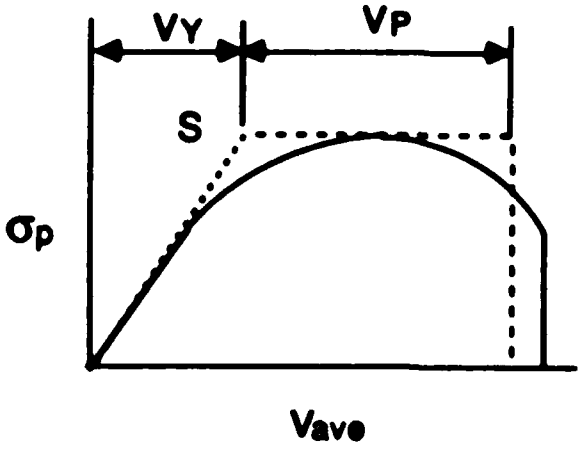

Fig. 8. Particle stress vs. average displacement

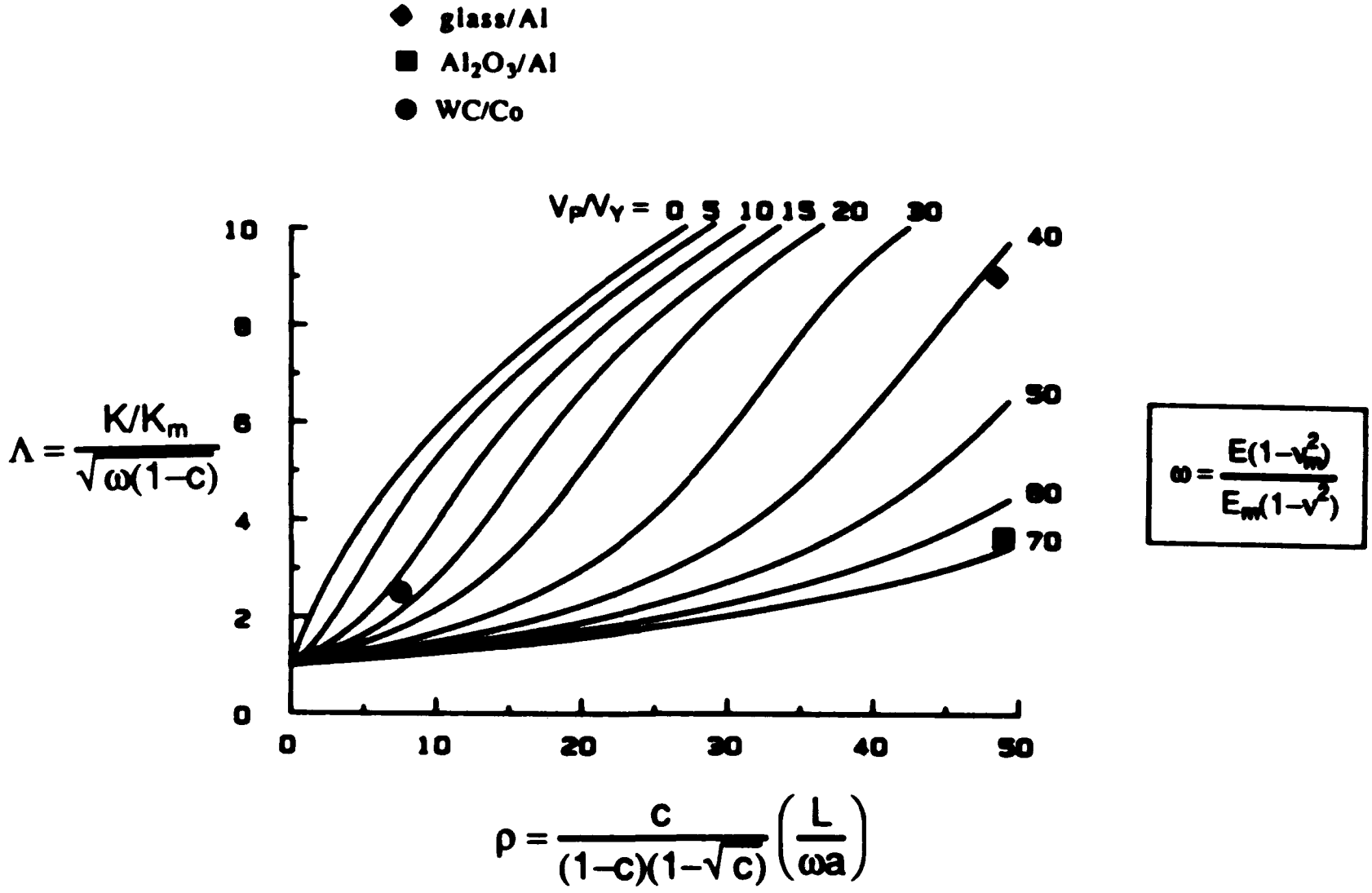

Fig. 9. Modified toughening ratio vs. non-dimensional bridge length

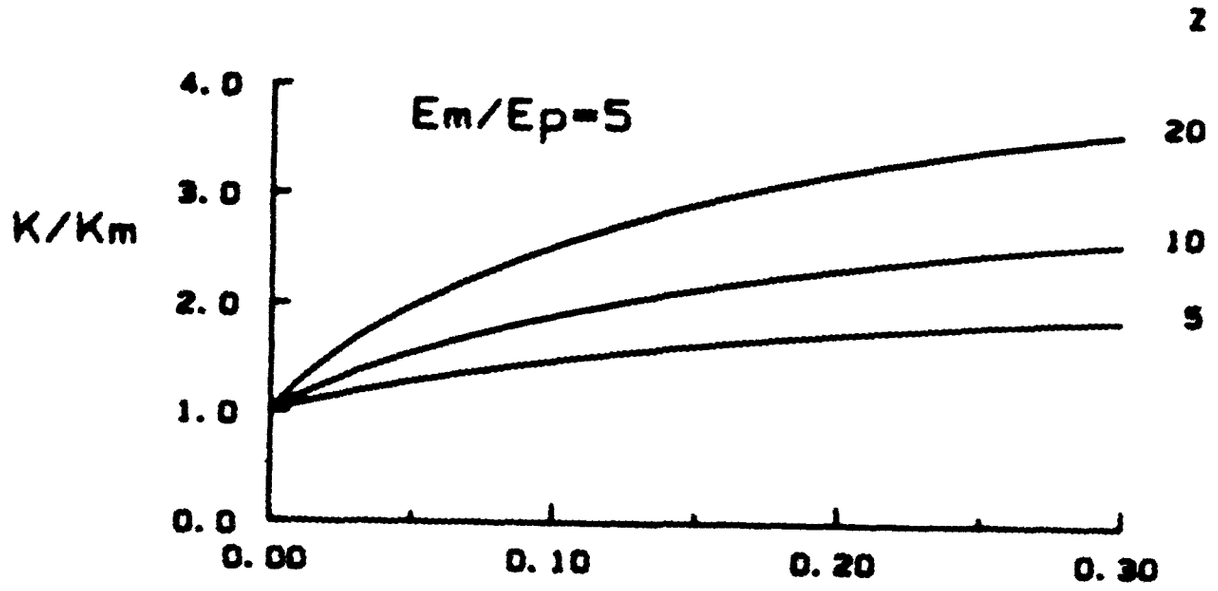

(a)

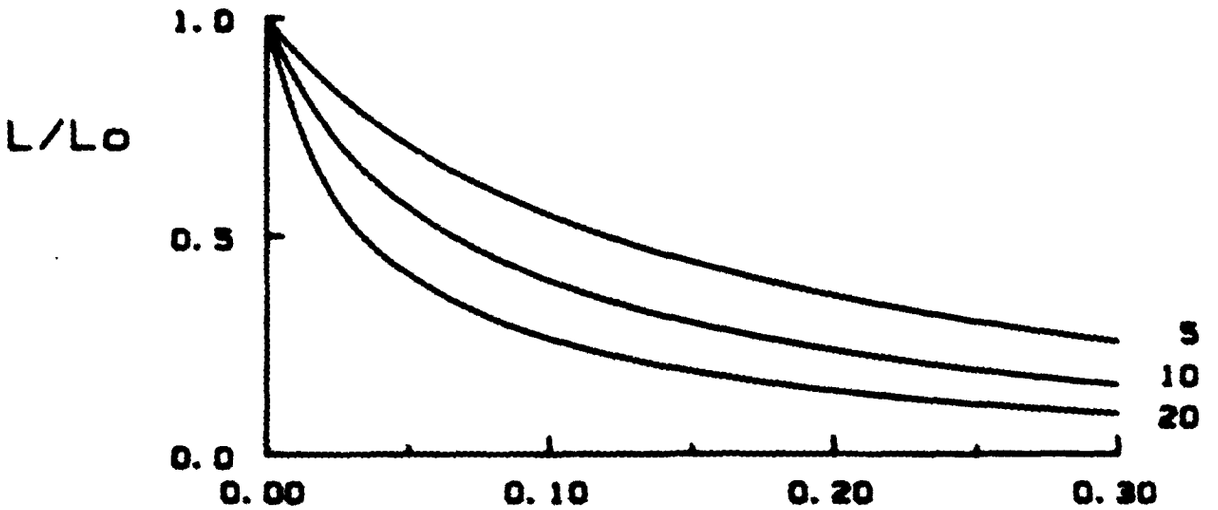

(b)

Fig. 10. Variation with particle concentration of (a) toughening (b) bridge length

END

9-87

DTIC